Effects of Mn, Al and Lattice Defects on the Thermoelectric Properties of $CrSi_2$

$CrSi_2$ の熱電特性における Mn, Al 及び格子欠陥が与える影響

Takahiro ORITA

折田 昂優

Kazuhiro ICHINO

一野 和寛

Keywords； $CrSi_2$, thermoelectric material, power factor, band structure, density functional theory

キーワード；$CrSi_2$，熱電材料，パワーファクター，バンド構造，密度汎関数理論

Abstract

Chromium disilicide ($CrSi_2$) is a p-type degenerate semiconductor, and its thermoelectric properties can be controlled by the substitution of Al or Mn. However, it has not been clarified why holes are the majority carriers in pure $CrSi_2$. In this study, $Cr_{1-x}Mn_xSi_2$ and $CrSi_{2-y}Al_y$ samples with x and y ranging from 0.00 to 0.20 were prepared and their thermoelectric properties were evaluated. The electronic density of states calculated by first-principles calculation based on density functional theory revealed that the atomic vacancies in the Si sites can supply holes.

二珪ケイ化クロム($CrSi_2$)は一般に p 型縮退半導体として知られており，その熱電特性は Al や Mn の置換によってコントロールできることが知られている．しかしながら，不純物を含まない純粋な $CrSi_2$ において正孔が多数キャリアを示す理由は明らかにされていなかった．本報告では，$Cr_{1-x}Mn_xSi_2$ 及び $CrSi_{2-y}Al_y$ 試料の x 及び y を 0.00 から 0.20 の範囲で変化させて作製し，その熱電特性を評価した．また，格子欠陥を考慮して密度汎関数法に基づく第一原理計算により電子状態密度を求めることにより，WDX により存在が示唆された Si サイト上の原子空孔が正孔を供給できることを明らかにした．

1. Introduction

Transition metal disilicides exhibit high power factors (PFs) at high temperatures. In addition, the abundance of constituent elements, large electrical conductivity, high-temperature stability, and corrosion resistance make them excellent thermoelectric material candidates[1]. Among the transition metal disilicides, $CrSi_2$ has attracted much attention because of its semiconducting properties[2]–[4] and excellent oxidation resistance in the high-temperature range of 700–1000 °C[5]. $CrSi_2$ is a hexagonal C40 crystal with space group $P6_222$, and it is a p-type degenerate semiconductor with a forbidden band width of 0.32 eV, but it has not been clarified what the carrier holes are derived from when $CrSi_2$ is undoped[6]–[9]. The PF of $CrSi_2$ is the highest at approximately 300 °C. However, at higher temperatures, the PF decreases as the Seebeck coefficient decreases owing to the bipolar effect, making it impossible to effectively regenerate waste heat from steel mills and nonferrous metal plants, where waste heat at 400–500 °C is common. Replacing the Si site with Al in the degenerate compound semiconductor $CrSi_2$ improves the PF by reducing the resistivity owing to the increased acceptor concentration, which changes the Fermi level to a lower position relative to the upper end of the valence band[9]–[12]. In the same way, substitution of Mn for Cr sites increases the concentration of electrons, which are minor carriers, generating an n-type semiconductor. We previously reported $CrSi_{2-y}Al_y$ (y = 0.00, 0.04, 0.08, 0.12, 0.16, 0.20)[13].

In this study, we investigated the electrical properties of $Cr_{1-x}Mn_xSi_2$ (x = 0.00, 0.04, 0.08, 0.12, 0.16, 0.20) and the crystal lattice changes before and after sintering, and we discuss the origin of the holes in undoped $CrSi_2$.

2. Materials and Methods

2.1 Material synthesis

Cr powder of 99.9% purity, Mn pellets of 99.9% purity, Si pellets of 99.999% purity, and Al pellets of 99.9% purity were weighed to obtain $Cr_{1-x}Mn_xSi_2$ (x = 0.00, 0.04, 0.08, 0.12, 0.16, 0.20) and $CrSi_{2-y}Al_y$ (y = 0.00, 0.04, 0.08, 0.12, 0.16, 0.20) in stoichiometric ratio. Each mixture was placed in a BN-coated alumina crucible and melted at 1500 °C in an Ar atmosphere of 4.0 atm using a multi-purpose high-temperature furnace (Fuji Dempa Kogyo Co., Ltd.) to synthesize polycrystalline ingots. The ingots were ground in an alumina mortar and sieved into powder using a 75 μm mesh. The powder was sintered by uniaxial hot pressing (HP) at 1175 °C and 39.2 MPa (400 kgf cm^{-2}) for 120 min in an Ar atmosphere of 4.0 atm. The lattice parameters were identified by X-ray diffraction (XRD) measurement of a portion of the sintered compact and the powder before sintering using a Cu Kα line at Rigaku Co. The detailed composition of the sintered compact was determined by scanning electron microscopy/wavelength dispersive X-ray analysis (SEM-WDX, JXA-8230, JEOL Ltd.).

2.2 Fabrication and characterization of the devices

After each sample was cut to a size of approximately 5 mm × 1.5 mm × 12 mm, the Seebeck coefficient S and specific resistance ρ were measured from room temperature to 500 °C under reduced pressure with a rotary pump. S was calculated by heating both ends of the sample with a heater and measuring the temperature and potential difference V at both ends of the sample using the equation

$$S = V/(T_H - T_L) \quad (1)$$

where T_H is the temperature at the high-temperature side of the sample and T_L is the temperature at the low-temperature side of the sample, set to a difference of 20 °C. The specific resistance ρ was calculated by the following equation using the four-terminal resistance measurement method:

$$\rho = V\, t\, w\, I^{-1}\, l^{-1} \quad (2)$$

where t is the thickness and w is the width of the sample. I is the value of the current flowing in the longitudinal direction of the sample, and it was set to 0.1 or 0.4 A. l is the distance between the terminals for measuring the potential difference in the longitudinal direction of the sample, which was 8 mm. V is the voltage.

The PF was obtained from the measured Seebeck coefficient S and specific resistance ρ using.

$$PF = S^2 \rho^{-1} \quad (3)$$

2.3 Electronic structure analysis by first-principles calculations

The electronic structures of $CrSi_2$, $CrSi_{1.96}\square_{0.04}$ with atomic vacancies at the Si site, and Al-substituted $CrSi_{1.926}Al_{0.074}$ and $CrSi_{1.8}Al_{0.2}$ were calculated from first principles using 2×2×3 supercells. For $CrSi_2$, the Cr and Si sites were completely occupied by Cr and Si, and atomic vacancies and Al atoms were partially introduced into the silicon sites. The calculations were performed with the cooperation of Professor Munetoh of Kyushu University.

3. Results and Discussion

3.1 Crystal structure analysis

The lattice constants a and c versus the Mn composition obtained from XRD measurements are shown in **Figs. 1** and 2. For the $Cr_{1-x}Mn_xSi_2$ sample (**Fig. 1**), the lattice constants a and c decreased with sintering, and the decrease rate of the lattice constants increased with increasing amount of Mn substitution. This suggests that the substitution of Mn in Cr sites was further promoted by HP sintering. The lattice parameters also decreased with increasing Mn substitution after HP sintering. Conversely, for $CrSi_{2-y}Al_y$ (**Fig. 2**), the lattice constants did not significantly change with HP sintering. This suggests that the substitution of Al in Si sites was complete at the end of melting. As the y value increased, a monotonically decreased, and c reached a maximum at y = 0.04 and decreased with a further increase in y (**Fig. 2b**). This is the same trend as that observed for samples prepared by HP in the range y = 0–0.1 [11].

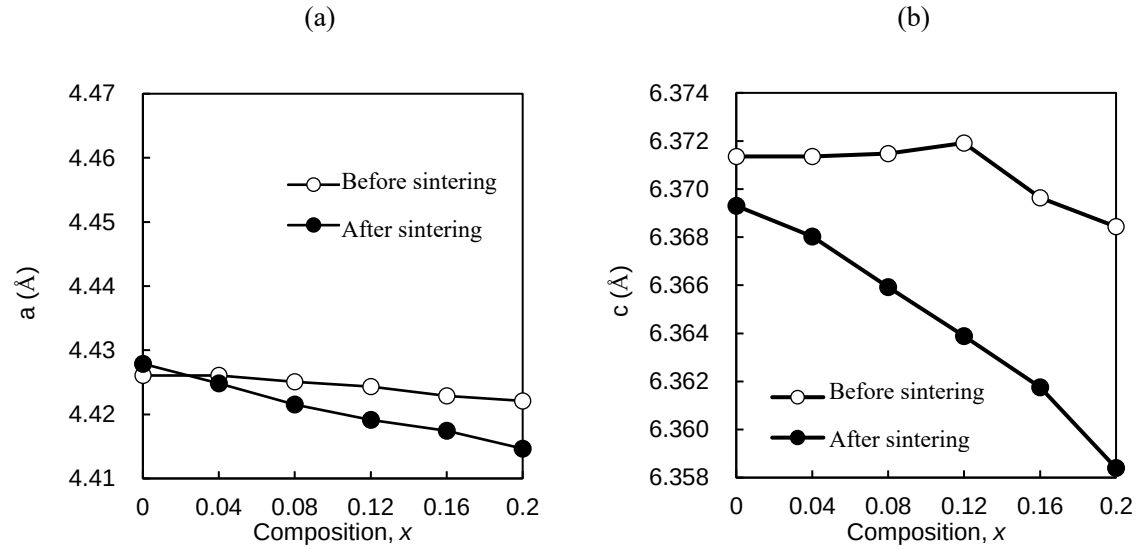

Fig. 1 Lattice parameters (a) *a* and (b) *c* of $Cr_{1-x}Mn_xSi_2$ versus the Mn preparation composition (x = 0.00–0.20).

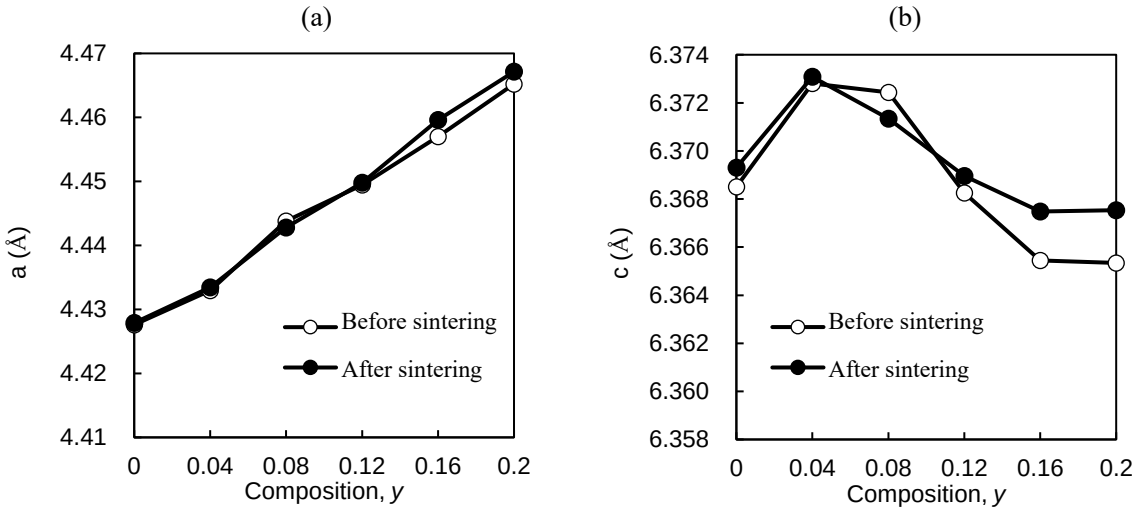

Fig. 2 Lattice parameters (a) *a* and (b) *c* of $CrSi_{2-y}Al_y$ versus the Al preparation composition (y = 0.00–0.20).

3.2 Seebeck coefficient and resistivity measurement

The temperature dependence of the Seebeck coefficient and resistivity for each sample is shown in **Figs. 3** and **4**, in which the average temperature at both ends of the sample and the temperature at the center of the sample are the x axis, respectively. For the $Cr_{1-x}Mn_xSi_2$ sample, the Seebeck coefficient was positive for $x \leq 0.08$, indicating that it is a p-type semiconductor. The sample with $x = 0.20$ showed negative values over the entire temperature range, indicating that it is an n-type semiconductor. The Seebeck coefficients of the samples with x = 0.12 and 0.16 were negative at room temperature, indicating n-type behavior, whereas the absolute values of the Seebeck coefficients decreased with increasing sample temperature, and the sign reversed above 200–300 °C, indicating p-type semiconductor behavior. From these results, it can be inferred that the number of electrons increased as the amount of Mn substitution increased. The samples with x = 0.12 and 0.16 showed very large

resistivity (**Fig. 4**), suggesting that they are intrinsic semiconductors with approximately the same number of electrons and holes. As the sample temperature increased, the number of holes increased more than the number of electrons, which possibly caused the p-type behavior of the Seebeck coefficient. The samples with x = 0.00 and 0.04 exhibited very small resistivity values (**Fig. 4**). The values tended to increase similarly with increasing temperature. For normal semiconductors, the resistivity decreases as the carrier concentration increases with increasing temperature. In contrast, the resistivity of degenerate semiconductors with high carrier concentration increases with increasing temperature because the effect of the lattice vibration is dominant, as in metals. From this fact, the samples with x = 0.00 and 0.04 are considered to be degenerate semiconductors. The sample with x = 0.08 exhibited the highest resistivity. This indicates that the sample with x = 0.08 had the lowest carrier concentration, and it is considered to be an intrinsic semiconductor. This is consistent with the large Seebeck coefficient. For $x \geq 0.12$, the resistivity tended to decrease with increasing amount of Mn substitution. This is due to the contribution of Mn as a donor, which is consistent with the Seebeck coefficient measurements.

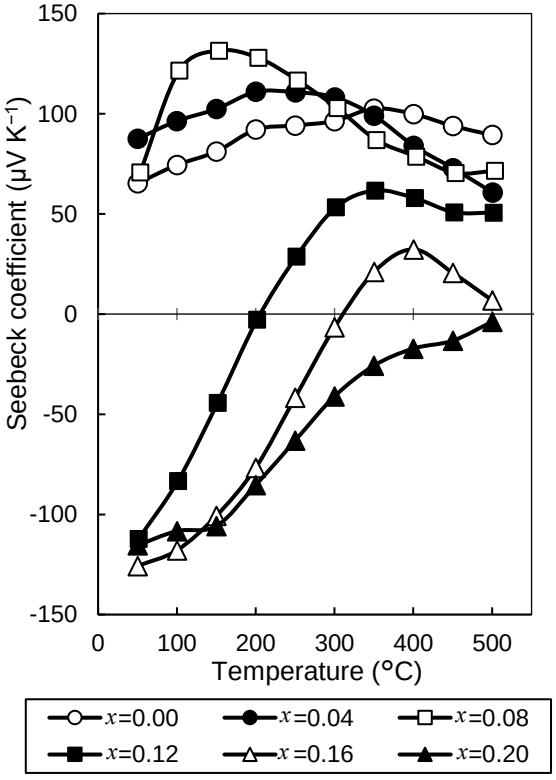

Fig. 3 Temperature dependence of the Seebeck coefficient for the $Cr_{1-x}Mn_xSi_2$ samples (x = 0.00, 0.04, 0.08, 0.12, 0.16, and 0.20).

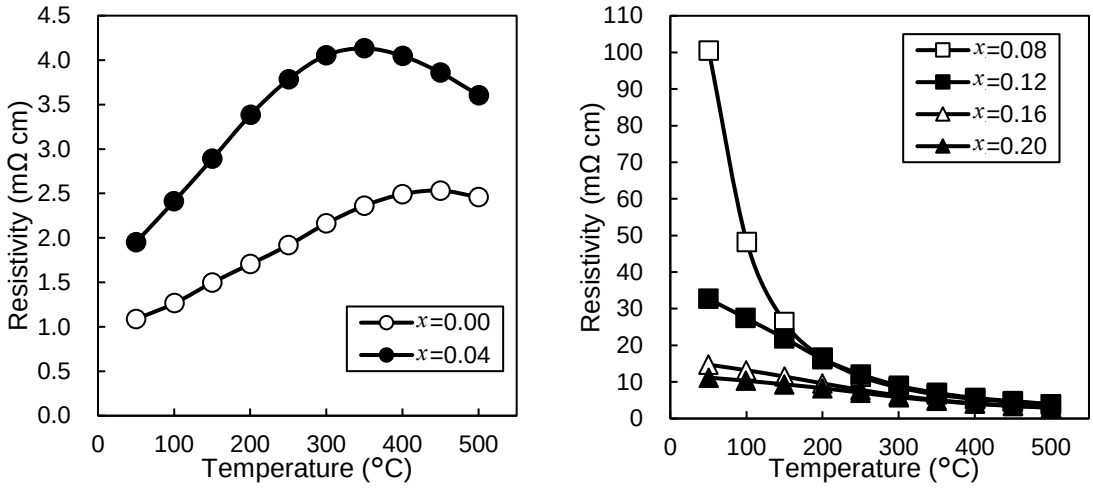

Fig. 4 Temperature dependence of the resistivity for the $Cr_{1-x}Mn_xSi_2$ samples (x = 0.00, 0.04, 0.08, 0.12, 0.16, and 0.20).

The Seebeck coefficients of the $CrSi_{2-y}Al_y$ samples were all positive, confirming that these samples are p-type semiconductors. The Seebeck coefficient was the highest for the sample with y = 0.00 and decreased with increasing Al substitution. This suggests that the carrier concentration increased with increasing Al substitution. For some of the samples, the Seebeck coefficient decreased in the high temperature range above 400 °C. This may be due to the bipolar effect. In particular, the Al-substituted samples with y = 0.08 or lower still exhibited a large Seebeck coefficient above 400 °C owing to the low carrier concentration, while the Al-substituted samples with $y \geq 0.12$ showed a decrease in the Fermi level, and they are thus less susceptible to the bipolar effect. The higher carrier concentration of the Al-substituted samples results in a smaller Seebeck coefficient. The resistivity decreased with increasing Al substitution amount y (**Fig. 6**). As for the Seebeck coefficient results (**Fig. 5**), this may be due to the increase in the carrier concentration. For all of the samples, the resistivity increased with increasing temperature, suggesting that all of the $CrSi_{2-x}Al_x$ samples are degenerate p-type semiconductors with high carrier concentration.

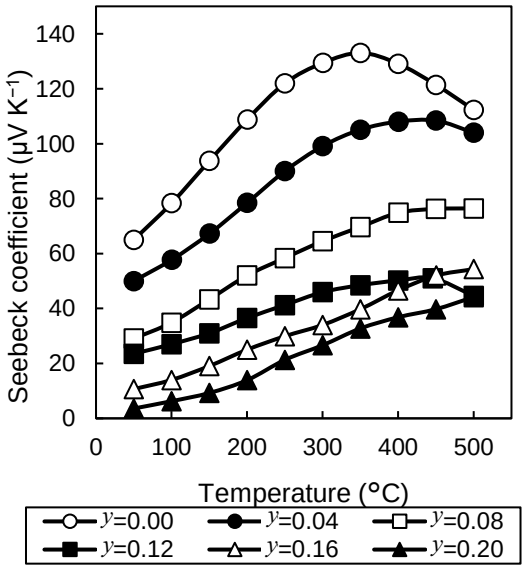

Fig. 5 Temperature dependence of the Seebeck coefficient for the $CrSi_{2-y}Al_y$ samples (y = 0.00, 0.04, 0.08, 0.12, 0.16, and 0.20).

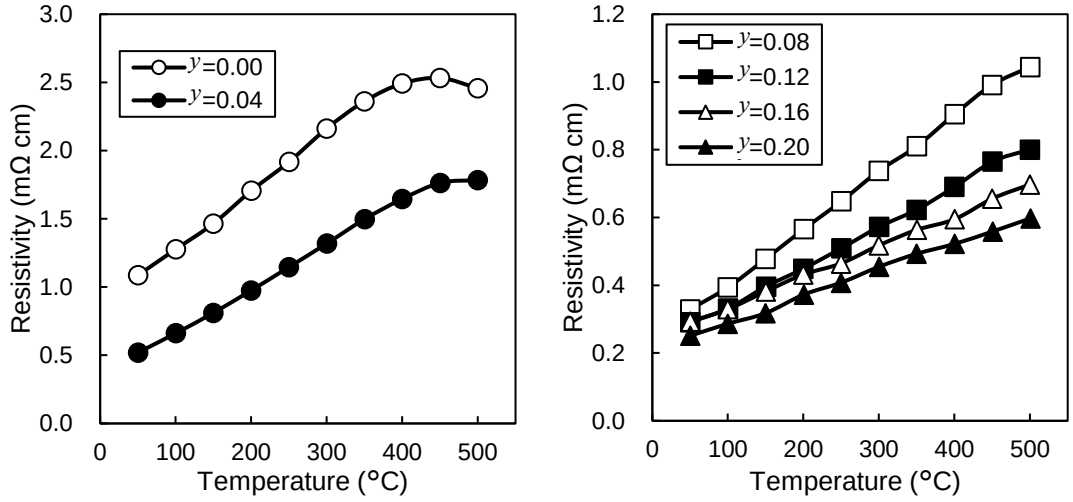

Fig. 6 Temperature dependence of the resistivity for the $CrSi_{2-y}Al_y$ samples (y = 0.00, 0.04, 0.08, 0.12, 0.16, and 0.20).

The correlation between the PF and temperature calculated using the electrical properties of each sample is shown in **Fig. 7**. The sample with x, y = 0.00, which had no elemental substitution, exhibited the best PF of 0.776 mW m^{-1} K^{-2} at 250 °C. The sample with y = 0.04 exhibited the highest PF in the high-temperature range above 400 °C. This is because of the more pronounced decrease in the Seebeck coefficient with increasing temperature for the x, y = 0.00 sample and the approximately 1.5 times higher specific resistance of the x, y = 0.00 sample when comparing the electrical properties of the x, y = 0.00 and y = 0.04 samples in the high-temperature range. Conversely, for the $Cr_{1-x}Mn_xSi_2$ samples, the PF value decreased with increasing Mn substitution. This is considered to be largely because the specific resistivity significantly decreased with decreasing carrier concentration and approached that of a true semiconductor.

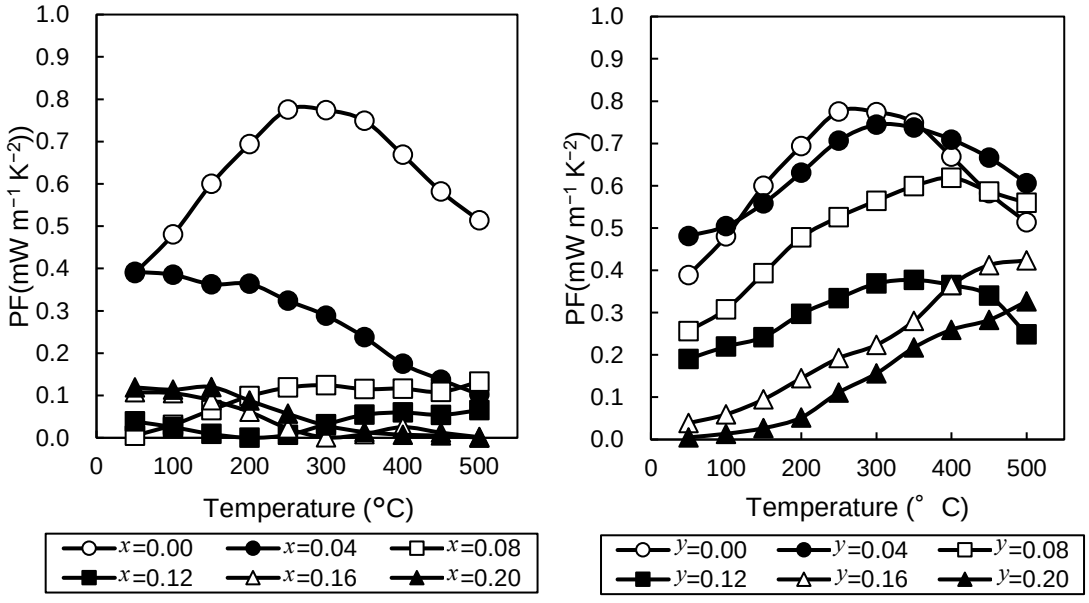

Fig. 7 Temperature dependence of the power factor for the $Cr_{1-x}Mn_xSi_2$ and $CrSi_{2-y}Al_y$ samples (x, y = 0.00, 0.04, 0.08, 0.12, 0.16, and 0.20).

3.3 Origin of the carriers

A more accurate composition of the matrix phase in $CrSi_{2-y}Al_y$ was obtained by WDX. The abundance ratio of each element and the stoichiometric ratios calculated so that Cr = 1 are given in **Table 1**. The abundance ratio of each element was determined by measuring five locations in the matrix and using the average of the three points excluding the maximum and minimum values. No elements other than Cr, Si, and Mn were detected in any of the $Cr_{1-x}Mn_xSi_2$ samples, and similarly no elements other than Cr, Si, and Al were detected in all of the $CrSi_{2-y}Al_y$ samples. For $CrSi_{2-y}Al_y$ samples, the sums of the stoichiometric ratios of Si and Al were less than 2 when the stoichiometric ratio of Cr was 1. This reduction is denoted □Si. Therefore, it is suggested that atomic vacancies may exist at the Si site, including in the undoped samples (x, y = 0.00).

Table 1 WDX results of samples prepared with compositions of $CrSi_{2-y}Al_y$ (y = 0.00, 0.04, 0.08, 0.12, 0.16, and 0.20).

y in $CrSi_{2-y}Al_y$	Chemical composition (%)			Stoichiometric ratio			
	Cr	Si	Al	Cr	Si	Al	□Si
0.00	34.5	65.5	N/A	1.00	1.90	0.00	0.10
0.04	34.1	64.5	1.4	1.00	1.89	0.04	0.07
0.08	33.9	63.1	2.9	1.00	1.86	0.09	0.05
0.12	34.2	61.7	4.1	1.00	1.81	0.12	0.07
0.16	34.4	60.3	5.4	1.00	1.75	0.16	0.09
0.20	33.8	59.2	7.0	1.00	1.75	0.21	0.04

From the results obtained from this experiment, the mechanism of the carrier generation in $CrSi_2$ is discussed. To computationally confirm that the carrier concentration increases with increasing Al substitution y in $CrSi_{2-y}Al_y$ and that the p-type behavior is also observed at y = 0, the electronic density of states were determined for three compositions, y = 0.00, 0.074, and 0.20, by first-principles calculations. WDX measurements suggested the presence of atomic vacancies at the Si site of the $CrSi_2$ crystal, suggesting that the stoichiometry was deficient. For larger Al substitution, the Fermi level is located at lower energy with respect to the upper end of the valence band, and the apparent band gap increases (**Fig. 8a**, **c**, and **d**). The apparent band gap, which is the difference between the lower end of the conduction band and the Fermi level in the valence band, increases with increasing Al substitution (**Fig. 8a**, **c**, and **d**). This suggests that the hole concentration increases with increasing Al substitution and the bipolar effect is suppressed, which is consistent with the results of the Seebeck coefficient (**Fig. 5**) and resistivity (**Fig. 6**) measurements. However, the calculated result for y = 0.00 (**Fig. 8a**) suggests that it is a true semiconductor, which is inconsistent with the measured result that suggested degeneracy. Conversely, the Fermi level of $CrSi_{1.96}□_{0.04}$ is located in the valence band (**Fig. 8b**). This suggests that the reason why pure $CrSi_2$ becomes a degenerate p-type semiconductor is the existence of atomic vacancies at the Si site, which contribute to the formation of holes.

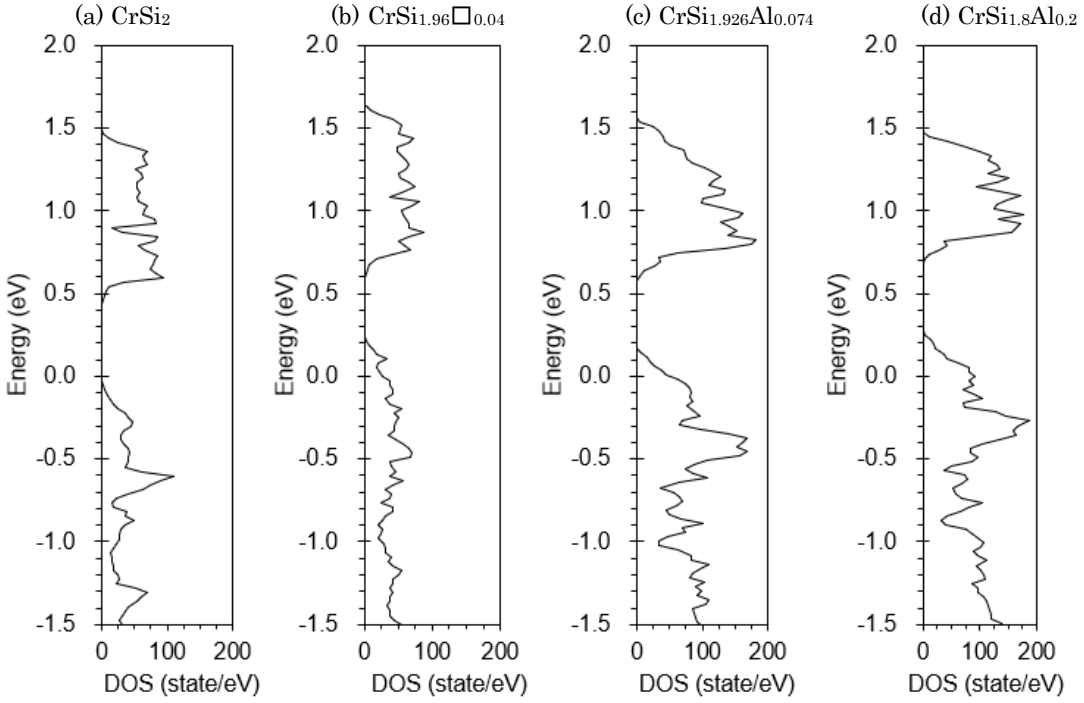

Fig. 8 Comparison of the density of states (DOS) near the Fermi level of $CrSi_2$ and its relatives obtained by first-principles calculations: (a) $CrSi_2$, (b) $CrSi_{1.96}\square_{0.04}$, (c) $CrSi_{1.926}Al_{0.074}$, and (c) $CrSi_{1.8}Al_{0.2}$

4. Conclusions

The thermoelectric properties of $Cr_{1-x}Mn_xSi_2$ ($0.00 \leq x \leq 0.20$) and $CrSi_{2-y}Al_y$ ($0.00 \leq y \leq 0.20$) have been evaluated. The results showed that Mn functions as a donor and Al functions as an acceptor. The electronic density of states of crystals with and without atomic vacancies at the Si site, and for each of the Al-doped crystal models were determined by first-principles calculations. The results of these calculations and the measurements described above confirmed that Al doping increases the hole density. In the case of the $CrSi_2$ crystal without atomic vacancies, the Fermi level exists in the forbidden band, while in the case of $CrSi_{1.96}\square_{0.04}$ crystal with atomic vacancies, the Fermi level exists in the valence band, suggesting degeneracy. These results indicate that the reason why $CrSi_2$ is a degenerate p-type semiconductor even if undoped is the presence of atomic vacancies at the Si site, which act as acceptors.

References

[1] Vining, C. B., Thermoelectric Properties of Silicides, in CRC Handbook of Thermoelectrics, (1995), 277-286

[2] I. Nishida, Journal of Materials Science, 7.10, (1972), 1119-1124

[3] I. Nishida, T. Sakata, J Phys Chem Solids, 39, (1978), 499-505

[4] A. B. Filonov, I. E. Tralle, N. N. Dorozhkin, D. B. Migas, V. L. Shaposhnikov, G. V. Petrov, V. M. Anishchik, V. E. Borisenko, physica status solidi (b), 186(1), (1994), 209-215

[5] Ma, J., Gu, Y., Shi, L., Chen, L., Yang, Z., & Qian, Y, Journal of alloys and compounds, 376(1-2), (2004), 176-179

[6] Mattheiss, L. F., Physical Review B, 43(2), (1991), 1863.
[7] Dasgupta, T., Etourneau, J., Chevalier, B., Matar, S. F., & Umarji, A. M. Journal of Applied Physics, 103(11), (2008), 113516
[8] Pan, Z. J., Zhang, L. T., Wu, J. S., Scripta materialia, 56(4), (2007), 257-260
[9] Pan, Z. J., Zhang, L. T., Wu, J. S., Scripta materialia, 56(3), (2007), 245-248
[10] Suresh, P., and A. M. Umarji. American Institute of Physics, In AIP Conference Proceedings, 1349(1), (2011), 429-430
[11] Solomkin, F. Y., Novikov, S. V., Kartenko, N. F., Kolosova, A. S., Pshenai-Severin, D. A., Uryupin, O. N., Isachenko, G. N., Technical Physics, 61, (2016), 153-156
[12] Pandey, T., Singh, A. K., Rsc advances, 4(7), (2014), 3482-3486
[13] T. Orita, Y. Matsukawa, K. Ichino, M. Arita, S. Munetoh. 傾斜機能材料論文集, 36, (2023), 13-18